Investigating Foreshocks and Aftershocks: Temporal Correlations in Thermal Creep Dynamics

Sylvain Mortgat, Supervisor: Tom de Geus

June 16, 2024

1 Introduction

Elastic manifolds driven over a disordered pinning potential exhibit a depinning transition. When an external driving force surpasses a critical threshold, the system undergoes a transition from a pinned (immobile) state to a depinned (moving) state. This transition typically results in avalanche dynamics, characterised by rapid movements punctuated by periods of little to no motion, with separation both in space and time. Such depinning transitions are observed across a variety of physical systems. For instance, magnetic domain walls in ferromagnetic materials, geological fault lines, and crack propagation in brittle materials.

In the presence of non-zero temperature, thermal fluctuations induce a creep regime, where slow and continuous motion is exhibited even when the driving force is below the critical threshold. This regime is particularly interesting because the collective dynamics display spatio-temporal patterns similar to those observed in earthquakes. In particular, they seem to exhibit aftershock-like sequences [1, 2].

In this report, we investigate the temporal correlations in the creep regime of a driven disordered system. The primary objective is to determine whether the considered system exhibits behaviour that gives rise to aftershocks. To this end, the temporal data representing the failure times of the system's components is analysed. Section 2 outlines the model used to generate the time series data. Section 3 describes how the system's activity is quantified and analysed across different experimental setups. The tools developed for analysing the data are openly accessible at https://github.com/sylvainshan/Time-Series.git.

2 Model

We consider a driven system as described in [3]: it is a d-dimensional cubic lattice with L^d blocks (sites). Each block, denoted as i, is characterised by a yielding threshold f_i^y and is subject to a force f_i that consists of two terms. The first is elastic in nature and only comes from neighbouring sites. The second comes from a driving force f. A block's stability is governed by its distance to yielding $x_i := |f_i| - f_i^y$ that corresponds to an activation barrier $E_i := |x_i|^\alpha \, \text{sign}(x_i)$, with $\alpha > 0$. At a finite temperature $T > 0$, the time of failure τ is exponentially distributed $\rho(\tau) = \frac{1}{\tau_i} \exp(-\tau/\tau_i)$. Thus, the mean failure time is $\tau_i = \tau_0 \exp(E_i/T)$ if the site is stable ($x_i \geq 0$) and $\tau_i = \tau_0$ if it is not ($x_i < 0$). When a block fails, its force drops to a small random value $f_i(t + \tau_i) = \varepsilon = f_i(t) - \Delta f_i$. The force drop Δf_i is uniformly redistributed to the 2^d nearest neighbours of i. In addition, a new yielding threshold f_i^y is sampled from a given distribution.[1] Finally, the position of the block is updated as $u_i(t + \tau_i) = u_i(t) + \Delta f_i/k$, where k denotes the elastic constant. The driving force is constant at all time since all force drops are always entirely redistributed. It is given by $f = \sum_i f_i / L^d$ and is set to $f_c/2$. Here, f_c corresponds to the critical force at which the interface undergoes a depinning transition at $T = 0$.

Implementation details The cellular automaton is implemented with the `GooseEPM` package [4]. We consider a $d = 2$ dimensional instance of the `SystemThermalStressControl` class with linear size $L = 512$ at a temperature $T = 0.002$. We set $\alpha = 3/2$, $\tau_0 = 1$, $k = 1$ and use the `laplace_propagator` for nearest neighbour interactions. The yielding threshold of each block, f_i^y, is sampled from a normal distribution with a mean 1 and a standard deviation 0.3. Upon failure, the force drops to a small ε which is also drawn from a normal distribution with a mean 0 and a standard deviation 0.01. The constant driving force f is set to $0.3 \approx f_c/2$. The critical force f_c is established by driving the system athermally and quasi-statically using a weak spring. During system initialisation, each block is assigned a force f_i sampled from a normal distribution with a mean f and a standard deviation 0.1. The system is iteratively updated by failing unstable blocks until all blocks are stable. To reach a steady state, the dynamics are run for $100L^d$ steps. Subsequently, data is collected in segments of $n_{\text{steps}} := 20L^d$ steps for analysis. The position and time of failure of each failing block is tracked throughout the event-driven simulation.

---

[1] See the implementation details.

3 Measurements

3.1 Relaxation time

The macroscopic relaxation time of the system, τ_α, is defined as the time needed to fail half of the system, i.e., $L^d/2$ different blocks. In practice, τ_α is obtained by running the system's dynamics over $190n_{\text{steps}}$ steps. Each time the count of distinct blocks that have failed exceeds $L^d/2$, we record the corresponding time, reset the count and measure the time until the next occurrence of $L^d/2$ block failures. Averaging over the measurements yields $\tau_\alpha \approx 5.91 \times 10^{135}$. In the following, time will be expressed in units of τ_α.

3.2 Activity measurements

From a time series $\mathcal{T} := \{t_{\text{e},i}\}_{i=1}^{n_\text{e}}$ comprising n_e events representing the block failure times, the cumulative function of these events is defined as

$$N(t) := \sum_{i=1}^{n_\text{e}} \Theta(t - t_{\text{e},i}), \qquad (1)$$

where Θ denotes the Heaviside function. The activity, A, is the derivative of N, which analytically corresponds to a sum of Dirac deltas:

$$A(t) := \frac{\mathrm{d}N}{\mathrm{d}t} = \sum_{i=1}^{n_\text{e}} \delta(t - t_{\text{e},i}). \qquad (2)$$

In the following paragraphs, we present three measurements based on data collected over $320n_{\text{steps}}$ failure steps.

Activity around microscopic failures A microscopic failure event, i.e., a single block failure, is characterised by its occurrence time. To measure the activity around such events, n of them are randomly picked. For each event, the cumulative number of preceding and succeeding block failures over time is counted. Then, an average is computed over all samples. The number of events is calculated for n_t time windows $\{\Delta t_i\}_{i=1}^{n_t}$ logarithmically spaced between t_{start} and t_{end}.[2] The average activity is calculated by approximating the derivative of the average of N, denoted $\langle N \rangle$, using centred differences:

$$\langle A_i \rangle := \frac{\langle N(\Delta t_{i+1}) \rangle - \langle N(\Delta t_{i-1}) \rangle}{\Delta t_{i+1} - \Delta t_{i-1}}.$$

At the boundaries, forward and backward finite differences are used. The results obtained by averaging over 218 777 failure events are shown in Figure 1. The mean activity is observed to be completely symmetrical around these events. Two distinct regimes are

---

[2] The i-th time window is given by $\Delta t_i = t_{\text{start}}(t_{\text{end}}/t_{\text{start}})^{i-1/n_t-1}$.

identified: the first regime exhibits a power-law decay of activity with an exponent $\eta = 0.83$. The second shows a constant activity level that corresponds to a linear increase in the cumulative number of events. The transition between these two regimes occurs over timescales ranging from $10^{-4}\tau_\alpha$ to $10^{-2}\tau_\alpha$.
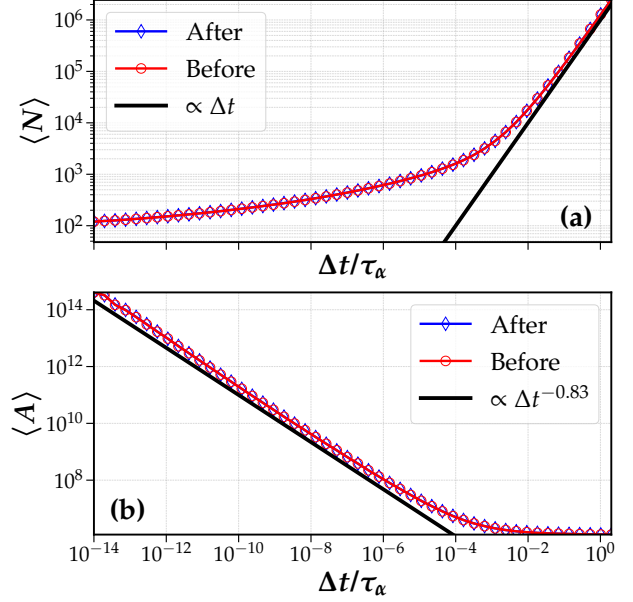

Figure 1: *(a) Mean cumulative number of events and (b) mean activity before and after 218 777 microscopic failure events with $n_t = 50$, $t_{\text{start}} = 10^{-14}\tau_\alpha$, and $t_{\text{end}} = 2\tau_\alpha$. The activity is symmetric and decreases as a power law with an exponent $\eta = 0.83$ before plateauing around $10^{-2}\tau_\alpha$. Events such that $t_{\text{e},i} - t_{\text{end}} < 0$ and $t_{\text{e},i} + t_{\text{end}} > \max \mathcal{T}$ are discarded.*

Coarsening the time series The discrete activity signal is convolved with a Gaussian kernel, denoted $K(t)$. This convolution yields a smoothed signal:

$$
\begin{aligned}
s(t) &= \int_{-\infty}^{\infty} K(\tau)A(t - \tau)\,\mathrm{d}\tau \\
&= \sum_{i=1}^{n_\text{e}} \int_{-\infty}^{\infty} K(\tau)\delta(t - \tau - t_{\text{e},i})\,\mathrm{d}\tau \\
&= \sum_{i=1}^{n_\text{e}} K(t - t_{\text{e},i}) \\
&= \frac{1}{\sqrt{2\pi\sigma_t^2}} \sum_{i=1}^{n_\text{e}} \exp\left(-\frac{(t - t_{\text{e},i})^2}{2\sigma_t^2}\right),
\end{aligned}
$$

which corresponds to a sum of Gaussians centred at the times of individual microscopic events. The temporal resolution, or characteristic time scale of the signal, is determined by σ_t. A smaller σ_t results in minimal overlap of the Gaussian functions, preserving individual event details. Conversely, a larger σ_t merges more events, highlighting broader trends. Essentially, σ_t controls the smoothing degree, allowing

the focus to shift from fine-grained to coarse-grained views of the system's activity. Thus, the value of s at any given time t reflects the system's activity on a timescale around t of the order of σ_t. Higher values of s indicate a greater number of events within this timescale. We use the local maxima of s as a measure of the size of a temporal cluster of microscopic events, i.e., as a measure of avalanche size.

Distribution of maxima Let $\mathcal{S} = \{S_i\}_{i=1}^{n_m}$ be the set of all local maxima of s. The distribution of avalanche sizes S computed with $\sigma_t = 3.15 \cdot 10^{-6} \tau_\alpha$ for 11 518 889 values is presented in Figure 2. A fit is calculated using the `powerlaw` package [5, 6]. It is observed that $P(S) \sim S^{-\tau_{exp}}$ with $\tau_{exp} = 1.30$ over approximately three orders of magnitude before a cutoff is reached. This exponent is close to the depinning exponent $\tau = 1.27$ identified in [3] for thermal avalanches. Such a similarity hints that the maxima of S encapsulate relevant information for the system.
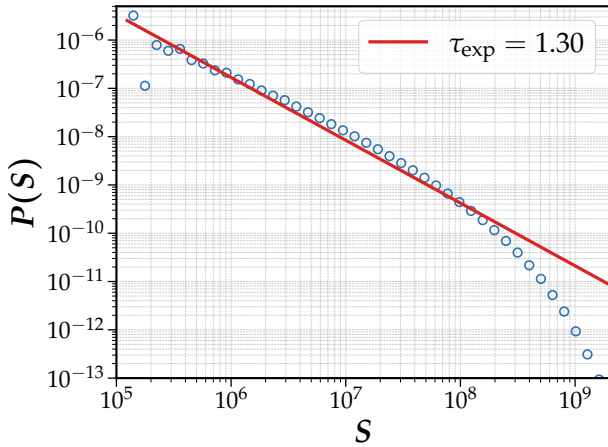

Figure 2: *Probability distribution $P(S)$ for local maxima S of the smoothed activity signal s with $\sigma_t = 3.15 \cdot 10^{-6} \tau_\alpha$. The data exhibits a power-law behaviour with an exponent $\tau_{exp} = 1.30$ consistent with the depinning exponent $\tau = 1.27$ found for thermal avalanches for the same system in [3].*

Activity around random S From the convolved signal, we create a subset of $\mathcal{S}$ made of n randomly chosen local maxima. By construction, the time of a local maximum t_E does not necessarily correspond to the time t_e of a block failure in the original time series $\mathcal{T}$. Therefore, for each maximum of S, the temporally closest microscopic event is considered as the initial time from which to count preceding and succeeding events. In other words, for each maximum, we find the time $t_o \in \mathcal{T}$ defined by

$$t_o = \arg \min_{t_e \in \mathcal{T}} |t_E - t_e| \, .$$

Once t_o is found, the procedure is the same as the measurement around randomly chosen microscopic events. The number of preceding and succeeding failures in $\mathcal{T}$ is counted over the same logarithmically spaced time windows. Then, an average over all samples is computed. The results obtained by averaging over 212 713 events are illustrated in Figure 3. For timescales greater than $10^{-2} \tau_\alpha$ the activity is symmetric and almost constant as in Figure 1 for randomly chosen block failures. Surprisingly, the activity is not perfectly symmetric for smaller timescales. On average, the activity decays faster after, and the cumulative number of events before is almost constant between $10^{-6} \tau_\alpha$ and $10^{-5} \tau_\alpha$. At first glance, this is not a trivial behaviour.
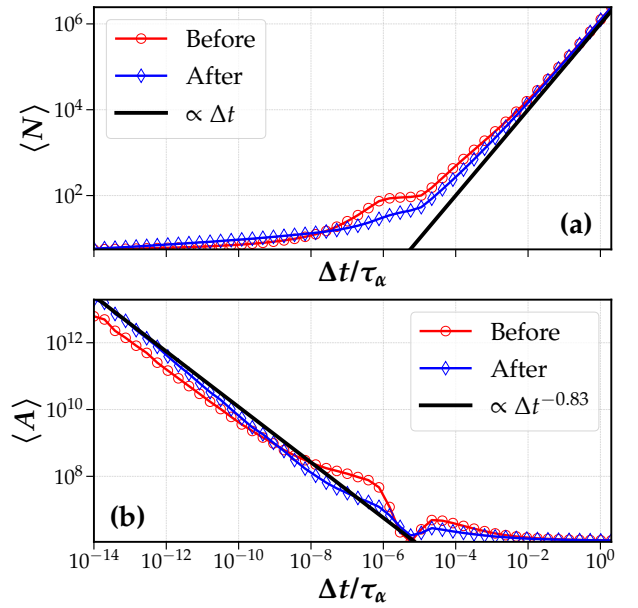

Figure 3: *(a) Mean cumulative number of events and (b) mean activity before and after 212 713 randomly chosen maxima in $\mathcal{S}$. Events are counted with $n_t = 50$, $t_{start} = 10^{-14} \tau_\alpha$, and $t_{end} = 2\tau_\alpha$. Events such that $t_{e,i} - t_{end} < 0$ and $t_{e,i} + t_{end} > \max \mathcal{T}$ are discarded. There is a slightly faster decay of activity following the peaks.*

Activity around similar S In previous measurements, the system's activity was observed around randomly selected events. By doing so, these measurements mixed significant events (large S) with minimal events (small S). Here, we compare the activity around avalanches involving a similar number of events. To achieve this, n_σ subsets of $\mathcal{S}$ are created, defined as:

$$\mathcal{S}_{n_\sigma} := \{S \in \mathcal{S} \mid S \in [\langle S \rangle + n_\sigma \sigma_S - \delta_{n_\sigma},$$
$$\langle S \rangle + n_\sigma \sigma_S + \delta_{n_\sigma}]\} \, ,$$

where $\langle S \rangle$ and σ_S are respectively the mean and the unbiased standard deviation of the values of $\mathcal{S}$; δS is

a small variation, and n_σ is an integer. In other words, we focus on local maxima of s that fall within intervals of size $2\delta_{n_\sigma}$ centred at $\langle S \rangle + n_\sigma \sigma_S$. After identifying these subsets, the same procedure is followed as for the unconditioned measurement of S. For each maximum, the closest time t_o in the original time series is found, and the activity before and after t_o is calculated. Table 1 lists the values of n_σ along with the number of samples in the corresponding set $\mathcal{S}_{n_\sigma}$. The variation is chosen as $\delta_{n_\sigma} = 0.05(\langle S \rangle + n_\sigma \sigma_S)$. Figure 4 illustrates the measurement results. As in the two other cases, the average activity over timescales greater than $10^{-2}\tau_\alpha$ is symmetric and constant for all values of n_σ. However, for shorter timescales, an asymmetry similar to that observed in Figure 3 is seen, with the activity before exhibiting a plateau that becomes more pronounced as the considered avalanche size increases (i.e., as S becomes larger).
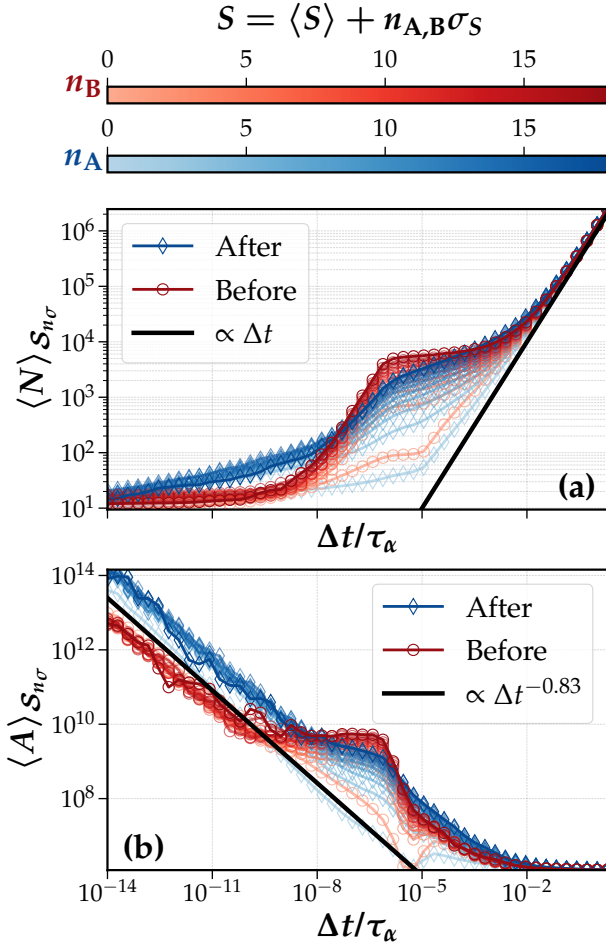
For $n_\sigma = 18$, a near "doubling" behaviour of the cumulative number of events is observed, alternating between slow growth (slope close to 0) and linear growth. The post-event activity is slightly smoother but also shows a period of quasi-constancy between $10^{-8}\tau_\alpha$ and $10^{-5}\tau_\alpha$. To better visualise these results, additional figures are provided in Appendix A.2. Figures 7a and 7b respectively show the activity before and after events of similar sizes. Figure 8 provides the activity results for each size individually.

n_σ	$|\mathcal{S}_{n_\sigma}|$
0	113 272
2	36 507
4	19 176
6	11 371
8	7 187
10	4 654
12	2 954
14	2 161
16	1 541
18	1 028

Table 1: *Number of samples for computing the mean activity around avalanches of similar sizes. $|\mathcal{S}_{n_\sigma}|$ denotes the number of elements in the set $\mathcal{S}_{n_\sigma}$.*

4 Conclusion

In this report, several measurements of activity were conducted. The first, concerning microscopic failures, showed a result that was completely symmetrical over time. Subsequently, the Gaussian convolution of the original activity allowed for the classification of avalanches by their sizes. This enabled two new measurements of activity: one by selecting avalanches of random sizes, and another by conditioning on the size of the avalanches. All measurements revealed symmetric and constant activity for time scales greater than $10^{-2}\tau_\alpha$. Measurements based on the convolved signal revealed non-trivial behaviour on time scales between $10^{-8}\tau_\alpha$ and $10^{-5}\tau_\alpha$. Finally, for time scales less than $10^{-10}\tau_\alpha$ all measurements show an activity decays that approximately follows as a power law with an exponent of 0.83. Beyond the activity measurements, analyses of the interevent-times could provide more insight into the system. Two very simple measurements of these interevent-time distributions are proposed in Figures 5 and 6 in Appendix A.1.

Figure 4: *Comparison of the system's activity around avalanches with similar sizes S. The colour gradients indicate the values of n_σ. (a) Mean cumulative number of events (b) mean activity. For timescales shorter than $10^{-10}\tau_\alpha$ and longer than $10^{-2}\tau_\alpha$, the activity behaviour is similar to the measurements in Figures 1 and 3, with a power-law decay $\langle A \rangle \sim \Delta t^{-\eta}$ with $\eta = 0.83$ at small timescales and a constant regime at larger timescales. The transition between these two regimes is asymmetric.*

References

[1] Ezequiel Ferrero et al. "Spatiotemporal Patterns in Ultraslow Domain Wall Creep Dynamics." In: *Physical review letters* 118 14 (2016), p. 147208. URL: https://journals.aps.org/prl/abstract/10.1103/PhysRevLett.118.147208.

[2] Ezequiel Ferrero et al. "Creep Motion of Elastic Interfaces Driven in a Disordered Landscape". In: *Annual Review of Condensed Matter Physics* (2020). URL: https://www.annualreviews.org/content/journals/10.1146/annurev-conmatphys-031119-050725.

[3] Tom W. J. de Geus, Alberto Rosso, and Matthieu Wyart. "Dynamical heterogeneities of thermal creep in pinned interfaces". In: (2024). arXiv: 2401.09830 [cond-mat.dis-nn].

[4] Tom W.J. de Geus. *GooseEPM*. https://github.com/tdegeus/GooseEPM. 2023.

[5] Jeff Alstott, Edward T. Bullmore, and Dietmar Plenz. "powerlaw: A Python Package for Analysis of Heavy-Tailed Distributions". In: *PLoS ONE* 9 (2013). URL: https://journals.plos.org/plosone/article?id=10.1371/journal.pone.0085777.

[6] Aaron Clauset, Cosma Rohilla Shalizi, and Mark E. J. Newman. "Power-Law Distributions in Empirical Data". In: *SIAM Rev.* 51 (2007), pp. 661–703. URL: https://epubs.siam.org/doi/10.1137/070710111.

A Appendix

A.1 Interevent-time distribution
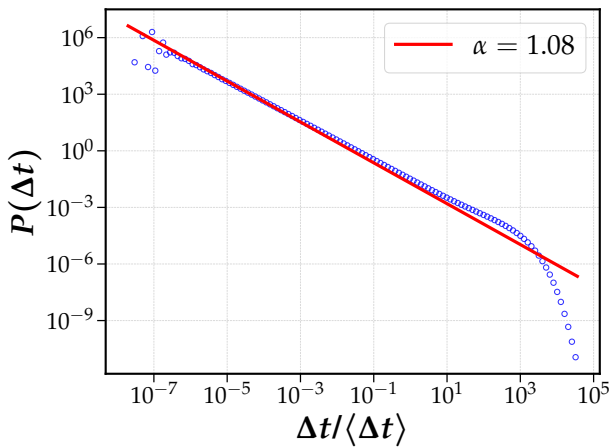

Figure 5: *Interevent-times of failure events $\mathcal{T}$ are power-law distributed with an exponent $\alpha = 1.08$. Here Δt denotes the time between two consecutive events, $\langle \Delta t \rangle$ is the mean interevent-time. This measurement is performed with $80 n_{\text{steps}}$ failure steps.*
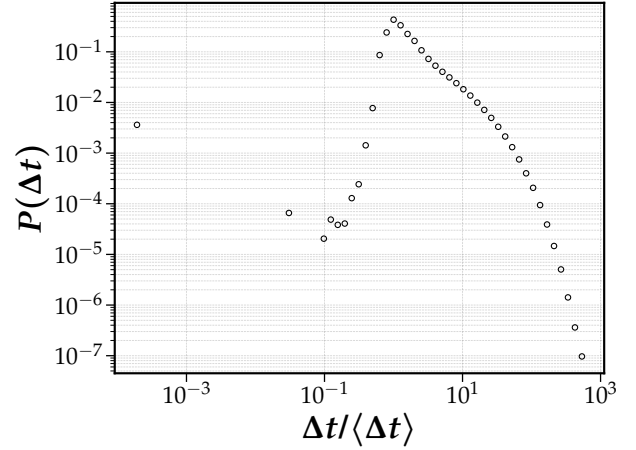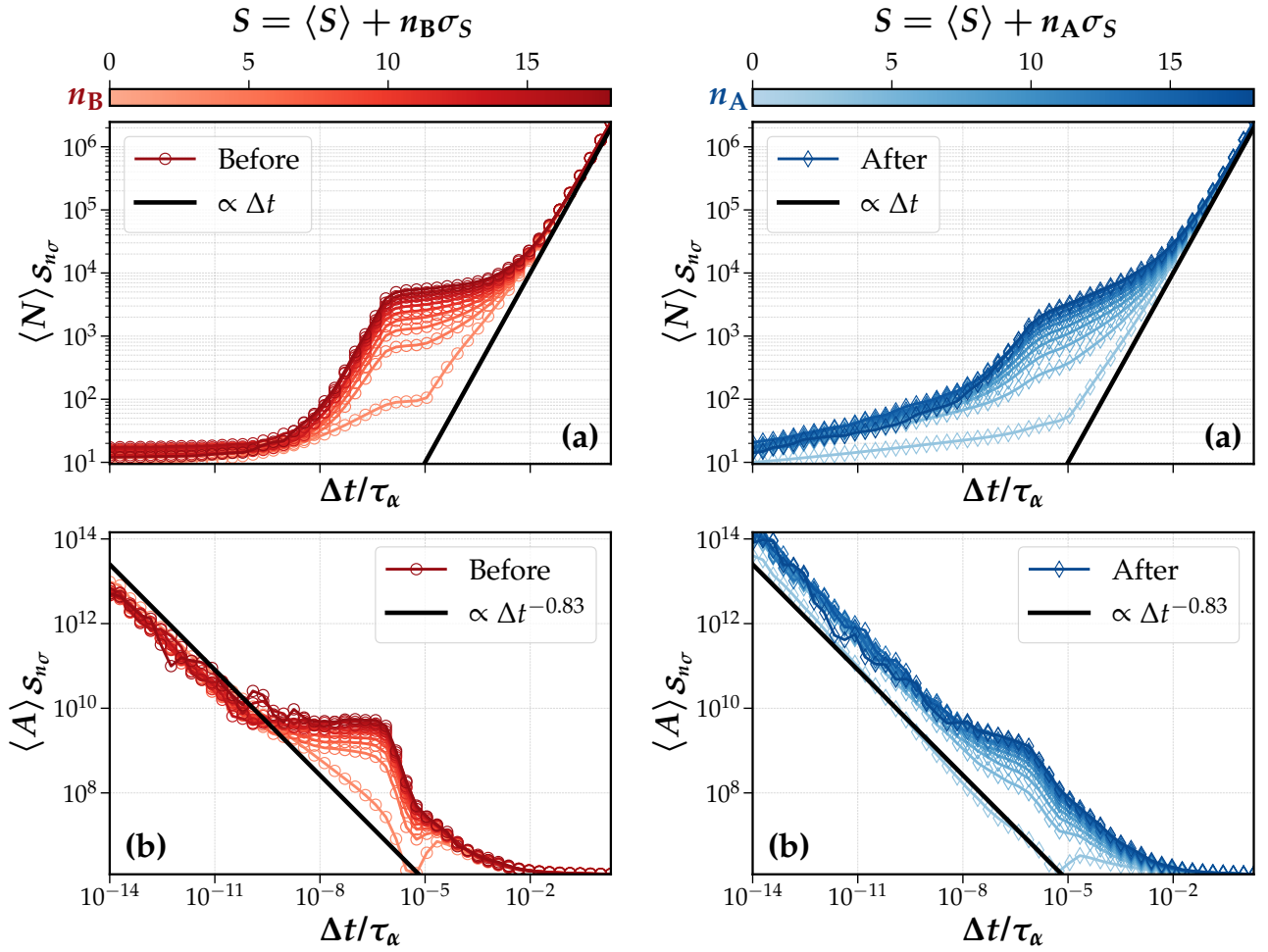

Figure 6: *Distribution of the interevent-times between the maxima of s computed with $2\,160\,543$ samples.*

A.2 Additional figures

The results obtaines in Figure 4 are represented differently in Figures 7 and 8 on the next two pages.

(a) *(a) Mean cumulative number of events (b) activity before avalanches of similar sizes. As S gets larger, the intermediate plateau becomes more pronounced. For $n_B = 0$, the activity has a local minima around $10^{-5}\tau_\alpha$ as in Figure 3.*

(b) *(a) Mean cumulative number of events (b) activity after avalanches of similar sizes. For $n_A = 0$, the activity decreases as in 3 with no intermediate regime. For larger avalanche sizes, it exhibits a portion with a lower decrease rate.*

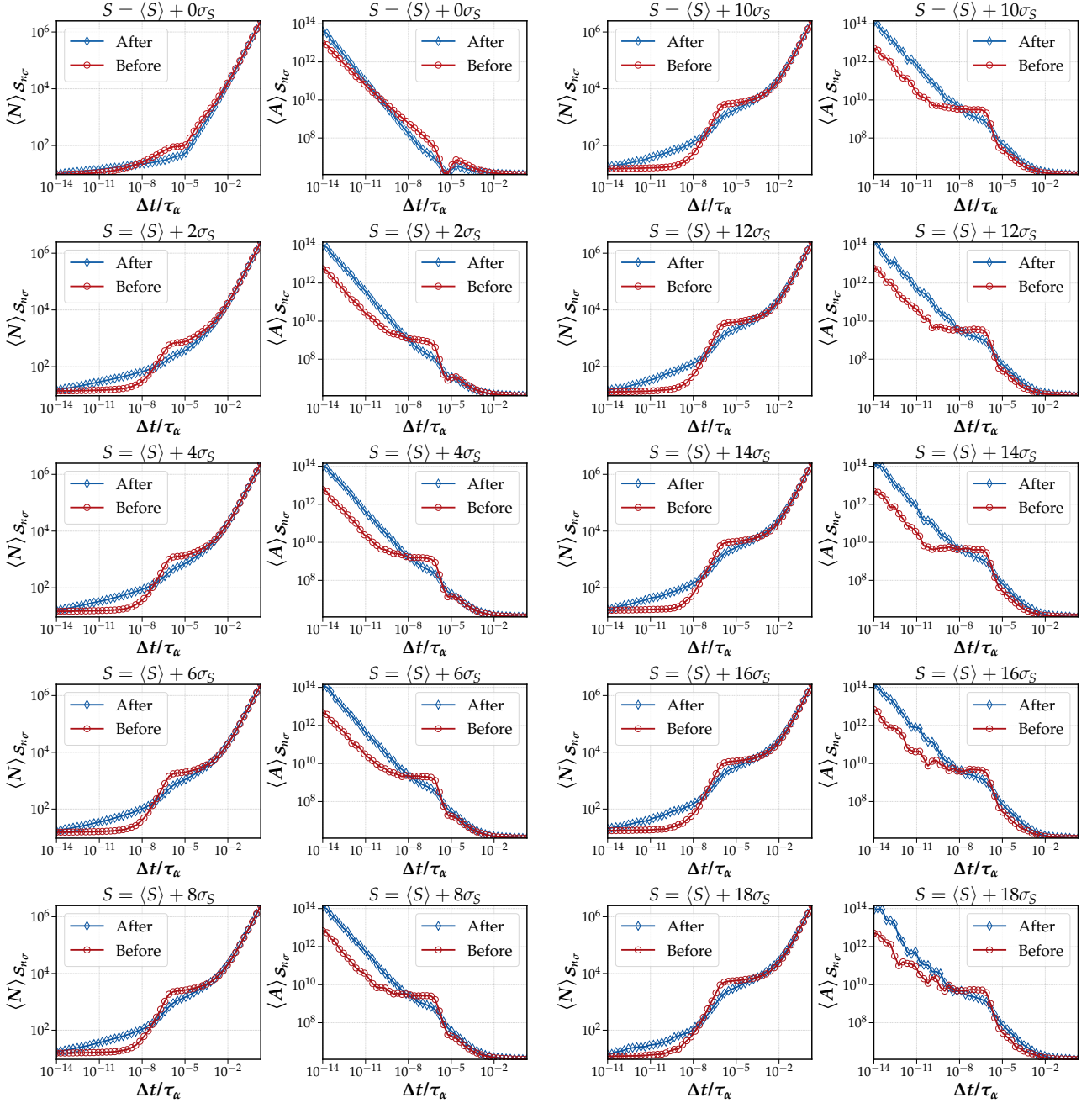**Figure 7:** *Mean activity evolution conditioned on avalanche size.*

Figure 8: *Mean cumulative number of events and mean activities for different avalanche sizes S.*